Data fusion of MEMS accelerometer and hydrostatic leveling for structural health monitoring – the test rig investigations

Leonhard Pleuger[1], Mario Haupt[2], Jens-André Paffenholz[1]

[1] Institute of Geo-Engineering, Clausthal University of Technology, 38678 Clausthal-Zellerfeld, Germany, (leonhard.pleuger@tu-clausthal.de; jens-andre.paffenholz@tu-clausthal.de)
[2] Glückauf Vermessung GmbH, 99706 Sondershausen, Germany, (m.haupt@glueckauf-vermessung.de)

Key words: *MEMS accelerometers; hydrostatic leveling; structural health monitoring; deformation measurement; sensor fusion*

ABSTRACT

This paper deals with the data fusion of MEMS accelerometer and hydrostatic leveling to contribute to the structural health monitoring, *e.g.*, of bridge structures. In the past years, researchers derived the deformation and bending line of bridges by profile measurements with terrestrial laser scanners (TLS), by means of MEMS accelerometers and image assisted total station (IATS) also with the aim to obtain the modal parameters (eigenfrequencies and eigenforms). At least the TLS-based approach is not suitable for a long-term monitoring. The approach by using MEMS accelerometers is very promising and allows for a long-term installation. Following the MEMS accelerometer approach, we investigate the data fusion of MEMS accelerometers and hydrostatic leveling, which also allows for a long-term installation of the monitoring system. This approach combines the classical hydrostatic leveling with its data showing long-term stability with the high-frequent data of the MEMS accelerometers. To investigate the data fusion of the abovementioned sensors a test rig is developed to simulate deformations in scaled laboratory environments. The test rig consists of a metal bar with a maximum span width of 3 m, which can be bent by a hydraulic press, and allows for a flexible positioning of both sensors. The scope of the laboratory experiments is the evaluation of different algorithms and methods regarding the data fusion, covering aspects of filtering and calculation of the bending line. Finally, those laboratory experiments should support the understanding and knowledge of the bending line calculations and performance of the used sensors to obtain deformation information with respect to specific load levels.

I. Introduction and Motivation

A. *Introduction*

Bridges are an essential part of our modern infrastructure. Following recent statistics (Statista, 2021) of, *e.g.*, German, highway bridges, one can see that a large number of bridge structures is barely acceptable or even worse (Figure 1). Because of their condition many of these bridges face reinforcement action or even replacement. Every construction work is associated with an enormous amount of costs and disturbances for the traffic and the people using the bridge. The goal of the reinforcement cycle is to maximize the bridges' operating time without compromising its structural integrity.

To quantify the structural integrity and the condition of the bridges, *e.g.*, in Germany, they are inspected regularly every six years according to DIN 1076. In addition to that, further inspections are conducted to have a snapshot of the recent situation every three years. By utilizing a monitoring system a high information density of the bridge parameters and their short-term changes can be obtained. This high information density allows a much more accurate prediction of the bridge behavior and therefore an optimal utilization of the load reserves and a prolonged reinforcement cycle. The main drawback of such monitoring systems seems to be their high costs for installation and operation, so that commonly such monitoring systems are taken into account when the bridge already shows significant damage. More cost-effective systems should be deployed at earlier stages in the bridge life cycle, while those sensor nodes could also support the establishment of digital twins, since real-time data from various sensor nodes is of great importance (Wenner *et al.*, 2021).

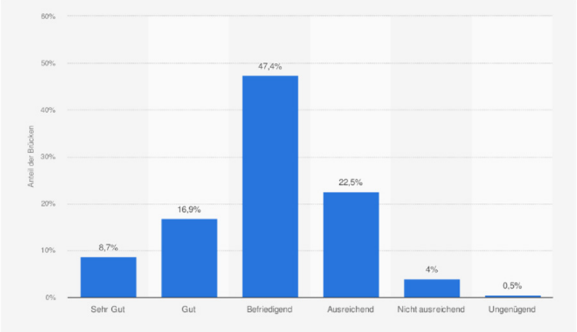

Figure 1. Condition of German highway bridges 2021 (Statista, 2021).

Conventional bridge monitoring systems often consist of classical geotechnical or geodetic sensors. Examples are inclinometers, hydrostatic leveling systems (Haupt and Hesse, 2019), total stations, and

GNSS measurements. These systems monitor different bridge parameters such as modal parameters (eigenfrequencies and eigenforms), bending line, or long-term deformation. The combination of aforementioned classical sensors as well as multiple low-cost or consumer grade sensors, *e.g.*, MEMS accelerometer, are well suited for an efficient acquisition of bridge parameters in the context of structural health monitoring (Omidalizarandi *et al.*, 2019).

B. *Related Work*

In the past years, researchers obtained the deformation and bending line of bridges by profile measurements with terrestrial laser scanners (TLS), or they obtained the eigenfrequencies and eigenforms by means of MEMS accelerometers and image assisted total station (IATS).

For instance, (Schill and Eichhorn, 2019) used a profile scanner to derive the vertical deformation of railroad bridges. The authors are calculating the deformation of bridge girders of a railroad bridge both as a bending line and as an oscillation at any point in the axis of the girder. In addition, they were able to obtain the amplitude spectrum of the bridge vibration. (Omidalizarandi, 2020) is determining the modal vibration parameters of a bridge using consumer grade MEMS accelerometers. An image assisted total station (IATS) is used for a 1D coordinate update (1D CUPT). (Štebe *et al.*, 2021) are calculating a 1D vibration trajectory in laboratory experiments using MEMS accelerometers supported by an IATS. Among other algorithms a Kalman filter was used for the data fusion of the acquired data.

For a long-term and extensive usage of these approaches for a bridge monitoring several challenges have to be overcome.

With respect to a cost-effective monitoring system the financial burden of the usage of at least one geodetic sensor (IATS or profile scanner) has to be considered:

- An IATS can only measure one point at a time. The acquisition of several measuring points has to be carried sequentially, which gains an importance to be considered for an increasing number of object points to be measured.
- A profile scanner can only capture deformations in a 2D profile. While increasing the spatial coverage by using classical TLS is an option, one will decrease the temporal resolution.

C. *Motivation of our approach*

The aim of our approach is to estimate bridge deformations in particular the vertical deformation to calculate a bending line as well as the oscillation in one point on the bridge girder.

In order to address this task and to avoid the aforementioned challenges due to permanent installations, a different approach will be presented here, which consists of a combination of a precise pressure based hydrostatic leveling and a consumer grade MEMS accelerometer. The combination of these two sensors offers the advantage that the IMU can capture vibrations and frequencies of the bridge girder, while the hydrostatic leveling can provide a 1D coordinate update. As long as the evaluation of the data is done in the local coordinate system of the hydrostatic leveling system no additional external geodetic sensor is required. The hydrostatic leveling allows an acquisition rate of more than 1 Hz. Furthermore, the sensor nodes can be arranged in any arbitrary three-dimensional grid as long as the height differences are within the measurement range of the hydrostatic leveling sensors.

On the one hand, the data analysis is possible in the position domain, *i.e.* metric deformation, where the focus is on the estimation of the bending line and the long-term deformation. On the other hand, the data can be analyzed in the frequency domain with the focus on the eigenfrequencies and eigenforms. The sensor fusion creates a surplus, since the stand-alone sensors either do not have sufficient long-term stability due to drift (accelerometer) or do not have the necessary acquisition rate (hydrostatic leveling).

Possible drawbacks of a combined measurement system are the costly installation of the sensors on the structure or the inertia of the hydrostatic leveling, against dynamic deformations. In addition, the use of consumer grade accelerometers affects the performance of the sensor and the accuracy of the system.

To investigate the potentials of the presented sensor combination the following points will be addressed:

1. Design of a test rig;
2. Evaluation of different data fusion algorithms in a single sensor node;
3. Transfer of the algorithm to additional sensor nodes and calculation of a bending line;
4. Validation of the results with a profile scanner or IATS;
5. Review of the proposed sensor combination and data fusion.

This contribution addresses the points one the design of a test rig and two the evaluation of different data fusion algorithms in a single sensor node.

II. The test Rig

A. *Design*

The goal of the test rig is to simulate at least one span of a bridge supported on two sides. This synthetic bridge is exposed to a load and the deformation resulting from the load measured by the sensor system.

The setup of the experiment can be described with the following principle sketch (Pleuger, 2020), (Figure 2).

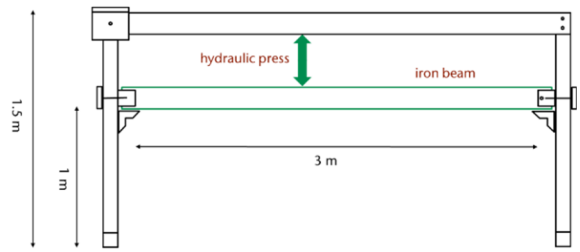

Figure 2. Principle sketch of the test rig with dimensions.

The test rig is a frame in which a beam supported on two sides can be installed. A hydraulic press is installed between the beam and the crossbar of the frame. The beam simulates a bridge girder and the hydraulic press is acting as a permanent load. In addition, an analog dial gauge is mounted next to the sensor node under consideration to validate the measured displacement (Figure 3).

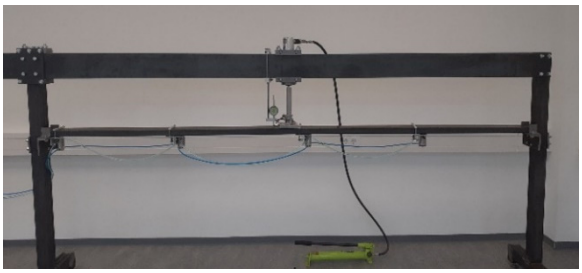

Figure 3. The test rig with applied sensor nodes.

It is possible to shift the force application point of the hydraulic press on the beam. In addition, the design of the stands and supports allows the use of different beams with different cross-sections and lengths with a maximum length of three meters.

The test rig concept is modular and thus it can be rearranged by:

1. Use of other/additional sensors, such as terrestrial laser scanner/profile scanner or IATS.
2. Extension of the synthetic bridge to several spans by installing another stand as a support.
3. Simulation of different (dynamic) loads to describe a bridge crossing more realistically.

B. *Choice of sensors and sensor application*

One selected sensor is the electronic pressure-based hydrostatic leveling system of the type PC-HAS4-500 from the company Position Control (Friedrichsthal, Germany). The measuring range is between 0 mm and 500 mm with an accuracy of $\max. 0.09\ \%FS$ as the sum of nonlinearity, hysteresis and repeatability. The long-term stability is $\min. 0.09\ \%FS/a$. The units of the hydrostatic leveling system are controlled via an RS-485 interface with ASCII protocol (Position Control, 2022).

The selected accelerometer is part of the IMU chip BNO 055 of the company Bosch. Here, the chip embedded in the modular system by the company Tinkerforge (Schloß Holte-Stukenbrock, Germany), in particular the IMU brick 2.0, is used. The Tinkerforge python API is used for the sensor control and data logging. The measuring range of the accelerometer is configured to $\pm 4\ g$ resulting in a 14 bit resolution with a maximum acquisition rate of 100 Hz. The non-linearity is specified by the manufacturer as $\max. 2\ \%FS$ and the output noise density is specified as $\max. 190\ \mu g/Hz$ (Bosch Sensortec, 2016). The suitability of this sensor for bridge monitoring has already been proven by, *e.g.*, (Kemkes *et al*., 2019).

The sensors are mounted on the test beam in sensor nodes. One sensor node consists of a hydrostatic leveling unit and a MEMS accelerometer, which are firmly connected to the test beam via an aluminum frame (Figure 4).

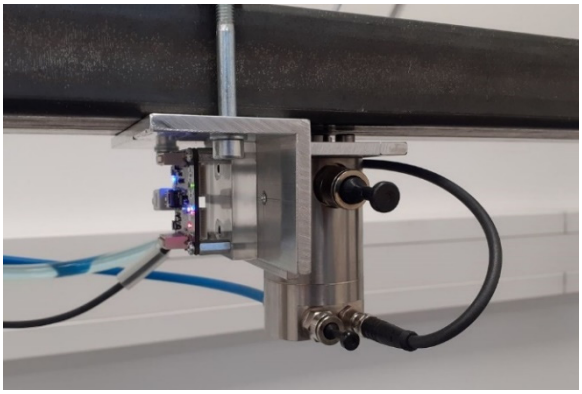

Figure 4. A Sensor node with MEMS accelerometer and hydrostatic levelling - MEMS accelerometer (left) and hydrostatic levelling unit (right); iron beam (top).

To investigate the measurement noise of the sensors, values were recorded over a period of one hour without any external load being applied. The results can be seen in Figure 5 and Figure 6 as the histograms of the captured data.

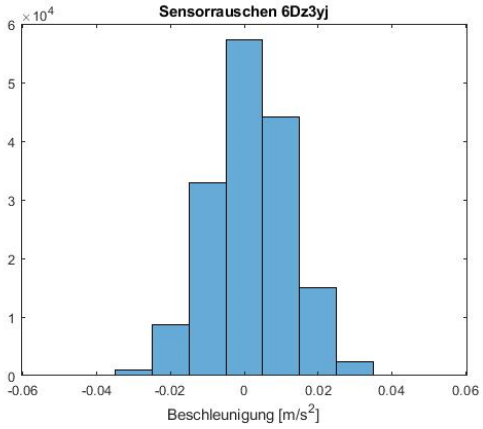

Figure 5. Histogram of the accelerometer (mean centred) for the measured accelerations.

The distribution of the measurements suggests an approximatly normal distributed noise. The classes of the accelerometer's histogram were chosen with

respect to the quantification steps of the accelerometer measurement. Table 1 gives an overview of the statistical parameters, which clearly indicate the difference in the sensor performance between hydrostatical leveling and consumer grade accelerometer.

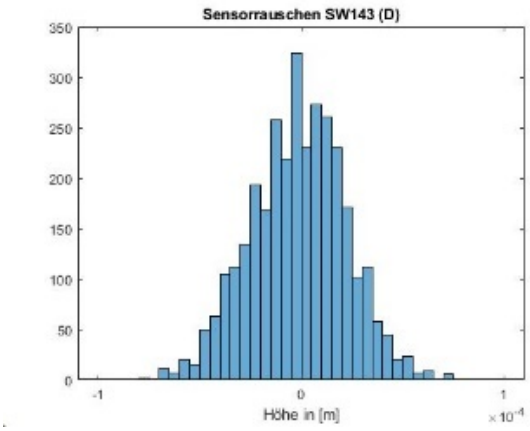

Figure 6. Histogram of the hydrostatic leveling (mean centred) for the measured height differences.

Table 1. Statistical parameters of measurement noise

Parameter	Hydrostatic leveling	IMU
Mean	$-1.55 \cdot 10^{-6} m$	$0.0026\ m/s^2$
Median	$-1.02 \cdot 10^{-6} m$	$0.0000\ m/s^2$
Standard deviation	$3.33 \cdot 10^{-5} m$	$0.0110\ m/s^2$

C. *Experiment*

The experiment performed is a static load test in which several load levels are applied. A dynamic load only occurs in the moment of load increase and decrease. The load test is subject to the following sequence:

1. *Initialization of the measurement*
2. *Beam for a few seconds at rest*: Based on the values measured during this time, the external acceleration influences of the accelerometer are subtracted and the deformation of the hydrostatic leveling unit is set to zero.
3. *Application of the load*: After the rest period, the hydraulic press is operated with a hand pump and the beam is loaded. After the pump has been operated for the first time, there is a pause of a few seconds to allow the hydrostatic leveling to adjust. After that, the hand pump is operated according to the same sequence until the desired maximum bending is reached. Each operation of the hand pump corresponds approximately to a deformation of 3 mm at the sensor node under consideration. The load applied by the hydraulic press is to be considered as a static load. No vibrations or overruns are simulated that would occur in a real structure.
4. *Maximum load*: The bridge beam remains in the maximum displacement state for a few seconds.
5. *Unloading*: The beam is unloaded via the hand pump. The beam returns to its initial position. The data acquisition is stopped after a fade-out time.

An example for the captured time series is shown in Figure 7 and Figure 8. The numbers in those figures correspond to the steps in the experiment sequence.

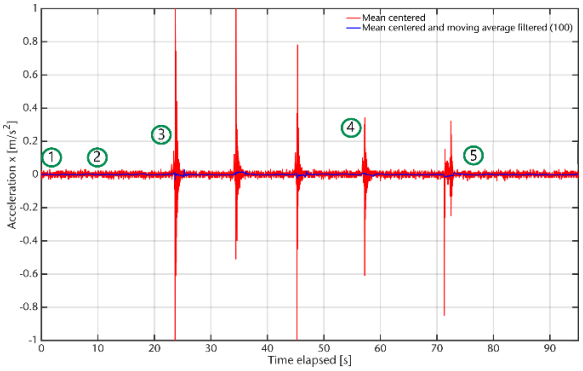

Figure 7. Timeseries of acceleration measurements. The peaks indicate a change of the applied load.

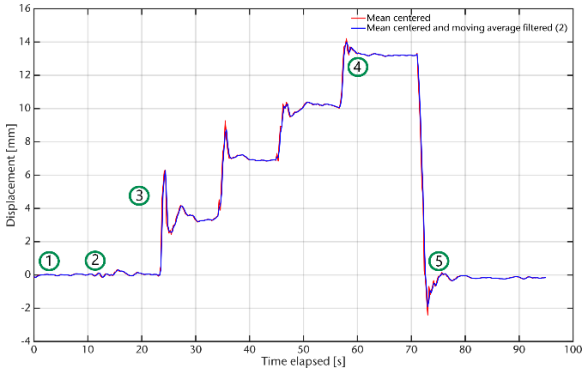

Figure 8. Timeseries of hydrostatic leveling unit measurements.

III. Data Processing

The data fusion between acceleration data and height differences, in the following named position data, is done with the help of a Kalman filter. In this paper, two Kalman filter based variants for data fusion are presented. Both variants have the 1D displacement, *i.e.* the vertical deflection, as parameter. The variant A fuses the position data with raw acceleration measurements. A numerical integration of the data is performed using the transition matrix of the filter. The variant B of the filter fuses the position data with the already double integrated acceleration data. Numerical integration is performed separately in selected ambient windows.

A consideration of a individual sensor calibration as well as corrections of temperature and atmospheric pressure is due to the controlled laboratory conditions neglected. The authors are aware of the importance of calibration and environmental parameter corrections which will both be considered in ongoing investigations. Possible approaches are presented by (Kemkes *et al.*, 2019) and (Štebe *et al.*, 2021).

A. *Kalman filter – Basics*

The Kalman filter was developed by Rudolf Emil Kalman in 1960. It has a great importance in the evaluation of dynamic time-dependent processes (Kalman, 1960).

The filter consists of a system model and an observation model. In the system model, a state vector k_{k+1} is predicted for epoch $k+1$ using the transition matrix and the state vector of epoch x_k (Eq. 1):

$$\hat{x}_{k+1}^{-} = T_{k+1,k} \cdot x_k^{-} + B_{k+1,k} \cdot u_k + S_{k+1,k} \cdot w_k \tag{1}$$

u_k and $B_{k+1,k}$ are the variables for the known input vector and its input gain. w_k and $S_{k+1,k}$ are the process error vector and its coefficient matrix.

In Equation 1 and the following equations, the superscript minus denotes the predicted value and the superscript plus denotes the filtered value.

The observation model describes the relationship between observations y_{k+1} and the state vector x_{k+1} with the measurement matrix H_{k+1}. v_{k+1} represents the vector of the measurement error (Eq. 2):

$$y_{k+1} = H_{k+1} \cdot x_{k+1} - v_{k+1} \tag{2}$$

In the filtering step, the system model and the observation model are merged using the Kalman gain K_{k+1} and the innovation i_{k+1} (Eqs. 3 and 4):

$$x_{k+1}^{+} = x_{k+1}^{-} + K_{k+1} \cdot i_{k+1} \tag{3}$$

$$\mathrm{i}_{k+1} = (y_{k+1} - H_{k+1} \cdot \hat{x}_{k+1}^{-}) \tag{4}$$

The Kalman gain is calculated by (Eqs. 5 and 6):

$$K_{k+1} = Q_{\hat{x}\hat{x}_{k+1}^{-}} \cdot H_{k+1}^{T} \cdot \left(Q_{ii,k+1}\right)^{-1} \tag{5}$$

$$Q_{ii,k+1} = Q_{yy_{k+1}} + H_{k+1} \cdot Q_{\hat{x}\hat{x}_{k+1}^{-}} \cdot H_{k+1}^{T} \tag{6}$$

where $Q_{\hat{x}\hat{x}_{k+1}^{-}}$ is the cofactor matrix of the predicted state and $Q_{yy_{k+1}}$ is the cofactor matrix of the observations. The cofactor matrix of the predicted state is (Eq. 7):

$$Q_{\hat{x}\hat{x}_{k+1}^{+}} = Q_{\hat{x}\hat{x}_{k+1}^{-}} - K_{k+1} \cdot Q_{ii,k+1} \cdot K_{k+1}^{T} \tag{7}$$

Thus, a recursive formulation for the filtered state vector and its associated cofactor matrix is obtained, see, *e.g.*, (Paffenholz, 2012).

B. *Kalman Filter variant A – acceleration and position*

Variant A of the Kalman filter was introduced by (Omidalizarandi *et al.*, 2019) and used by (Štebe *et al.*, 2021). Both used an IATS, similar to the hydrostatic leveling, to provide 1D displacement data.

The system model, introduced in Equation 1 is defined as follows, where $\bar{q} = 0.1$ is the ratio between the system and observation noise and Δt is the acquisition interval (Eq. 8):

$$\begin{bmatrix} z_{k+1} \\ v_{k+1} \\ a_{k+1} \end{bmatrix} = \begin{bmatrix} 1 & \Delta t & \frac{1}{2}\Delta t^2 \\ 0 & 1 & \Delta t \\ 0 & 0 & 1 \end{bmatrix} \cdot \begin{bmatrix} z_k \\ v_k \\ a_k \end{bmatrix} + S_{k+1,k} \cdot w_k$$
$$Q_{\hat{x}\hat{x}_{k+1}} = \begin{bmatrix} \frac{1}{20}\Delta t^5 & \frac{1}{8}\Delta t^4 & \frac{1}{6}\Delta t^3 \\ \frac{1}{8}\Delta t^4 & \frac{1}{3}\Delta t^3 & \frac{1}{2}\Delta t^2 \\ \frac{1}{6}\Delta t^3 & \frac{1}{20}\Delta t^2 & \Delta t \end{bmatrix} \cdot \bar{q} \tag{8}$$

The position data of the hydrostatic leveling and the acceleration data of the IMU are available as observations. Before the data fusion, the accelerations are filtered by a moving average with a filter length of 1 s to reduce the noise. Since the hydrostatic leveling unit collects data at a frequency of 2 Hz and the accelerometer collects data at a frequency of 80 Hz, the observation equation changes depending on which observations are present. When both observations are present, the following expression applies (Eq. 9):

$$\begin{bmatrix} z_{k+1} \\ a_{k+1} \end{bmatrix} = \begin{bmatrix} 1 & 0 & 0 \\ 0 & 0 & 1 \end{bmatrix} \cdot \begin{bmatrix} z_k \\ v_k \\ a_k \end{bmatrix} - v_{k+1}$$
$$Q_{yy_{k+1}} = \begin{bmatrix} \sigma_{HL}^2 & 0 \\ 0 & \sigma_a^2 \end{bmatrix} \tag{9}$$

σ_{HL} is the hydrostatic leveling's standard deviation obtained from the experiment sequence 2. σ_a is the standard deviation of the filtered acceleration signal.

If there is only one acceleration, then applies (Eq. 10):

$$[a_{k+1}] = [0 \quad 0 \quad 1] \cdot \begin{bmatrix} z_k \\ v_k \\ a_k \end{bmatrix}$$
$$Q_{yy_{k+1}} = [\sigma_a^2] \tag{10}$$

In addition to Kalman filtering, a Rauch Tung Striebel filter is applied to smoothen the time series (Rauch *et al.*, 1965).

C. *Kalman Filter variant B – integration and position*

In this variant B, the measured position of the hydrostatic leveling is fused with the dual integrated observations of the acceleration sensors.

Ambient windows are used to separate the acceleration time series in blocks with the relevant load signal. Load signals are identified as peaks in the acceleration time series that are greater than five times the calculated standard deviation. The size of the window is set to 0.5 s before the peak and 2 s after the peak (Figure 9).

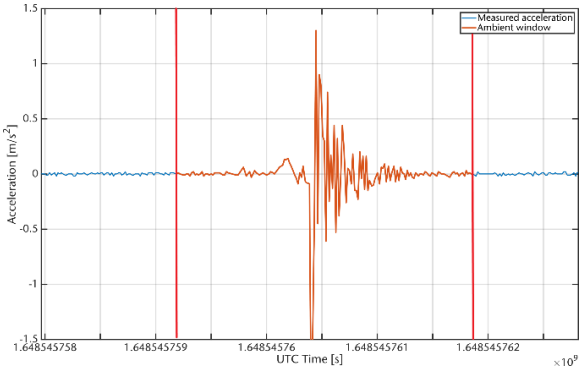

Figure 9. Selection of an ambient window – measurement noise (blue); ambient window raw acceleration (orange); limits of the ambient window (red).

To reduce the sensor drift induced by the numerical integration special integration algorithms have to be utilized. Possible integration methods of this signal would be a zero-phase filter (Štebe *et al.*, 2021), the method of the supporting polynomial (Resnik, 2014), the modeling of the acceleration time series and subsequent integration or the direct modeling of the deformations based on the acceleration (Gindy *et al.*, 2008).

The results shown here were obtained using the zero-phase filter method. Consideration of other integration algorithms and their comparison will be the subject of future work.

The integration algorithm of the zero-phase filter is shown in Figure 10. After each integration, a zero-phase filter is applied to eliminate the low frequency drift. The filter is a sixth order Butterworth filter with a cut off frequency of 0.2 Hz. In addition, a domain correction is applied after the first integration, considering the boundary condition $v_0 = v_{end}$ (Gindy *et al.*, 2007).

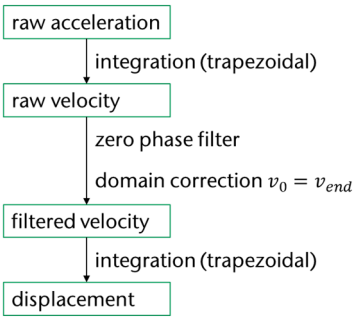

Figure 10. Integration algorithm - zero phase filter.

As a result of the selection of the ambient window and integration, the deformations are available in each of the ambient windows, where each ambient window starts with a deformation of zero (Figure 11).

1) The data fusion and Kalman filtering: The system model of this variant of the Kalman filter is defined as follows (Eq. 11):

$$\begin{bmatrix} z_{k+1} \end{bmatrix} = [1] \cdot [z_k] + S_{k+1,k} \cdot w_k$$
$$Q_{\hat{x}\hat{x}_{k+1}} = \bar{q} \tag{11}$$

The observation model must be adapted depending on which observations are available. A distinction is made between the following cases:

1. No observation (Eq. 12):

$$\begin{bmatrix} z_{k+1} \end{bmatrix} = [0] \cdot [x_{k+1}] - v_{k+1}$$
$$Q_{yy_{k+1}} = [0] \tag{12}$$

2. Hydrostatic leveling observation (Eq. 13):

$$\begin{bmatrix} z_{HL,k+1} \end{bmatrix} = [1] \cdot [x_{k+1}] - v_{k+1}$$
$$Q_{yy_{k+1}} = [\sigma_{HL}^2] \tag{13}$$

3. MEMS accelerometer observation (Eq. 14):

$$\begin{bmatrix} z_{pseudo,k+1} \end{bmatrix} = [1] \cdot [x_{k+1}] - v_{k+1}$$
$$Q_{yy_{k+1}} = [\sigma_a^2] \tag{14}$$

4. Both observations (Eq. 15):

$$\begin{bmatrix} z_{HL,k+1} \\ z_{pseudo,k+1} \end{bmatrix} = \begin{bmatrix} 1 \\ 1 \end{bmatrix} \cdot [x_{k+1}] - v_{k+1}$$
$$Q_{yy_{k+1}} = \begin{bmatrix} \sigma_{HL}^2 & 0 \\ 0 & \sigma_a^2 \end{bmatrix} \tag{15}$$

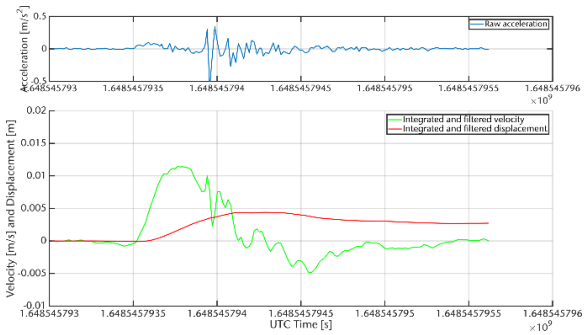

Figure 11. Numerical integration with ZPF Filter - acceleration (blue); velocity (green); displacement (red).

In Equations 14 and 15, the integrated accelerations are considered as a pseudo observation z_{pseudo}. To avoid accumulations of the integration error, a difference of the integrated accelerations is added to the last filtered state value (Eq. 16):

$$z_{integration,k+1} = z_k + \Delta z_{pseudo}$$
$$= z_k + \left(z_{pseudo,k+1} - z_{pseudo,k}\right) \tag{16}$$

IV. Results

Figure 12 and Figure 13 show the results of the data fusion using variant A, which has also been used by other researchers in differing scenarios with a combination between IATS and MEMS accelerometer. The input parameters are the mean-filtered acceleration measurements and the position data from the hydrostatic leveling. The variances of the measurement noise are used as cofactors.

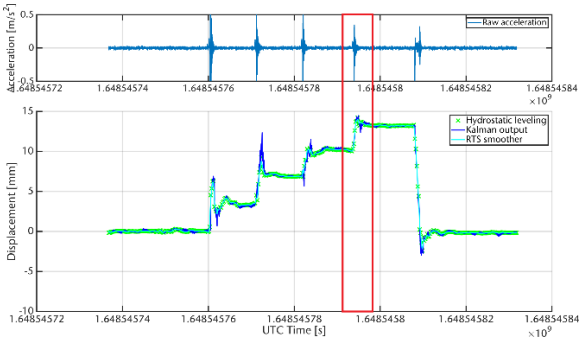

Figure 12. Result Kalman Filter variant A - Fusion of Acceleration with position – hydrostatic leveling (green); Kalman output (blue); RTS Smoother (cyan).

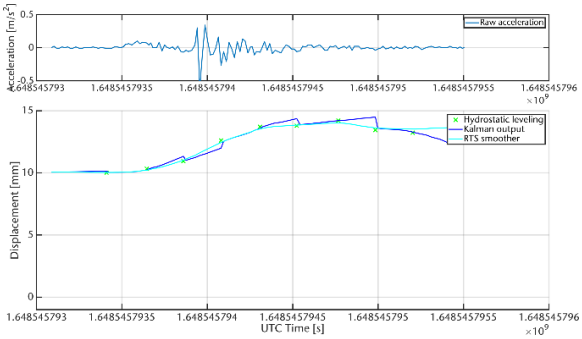

Figure 13. Result Kalman filter variant A – Selection. The Kalman output drifts in one direction until it is updated with a position measurement – hydrostatic leveling (green); Kalman output (blue); RTS Smoother (cyan).

It can be seen that the acquired time series mainly follows the hydrostatic leveling observations. However, especially in the moments of the load application strong oscillations can be seen. On the one hand, this is a result of the drift of the accelerometer, as shown in Figure 13. On the other hand, the oscillations are also caused by vibrations of the water column in the hydrostatic leveling unit, see Figure 12.

The result of the RTS filter strongly approximates the observations of the hydrostatic leveling, because of the standard deviation-based cofactors of the filter.

The results of filter variant B are shown in Figure 14 and Figure 15. It can be seen that the integrated ambient windows describe the deformation adequately in most cases. With the presented filter variant, it is possible to reduce the sensor drift of the MEMS accelerometer in the position domain as well as to significantly reduce the deviations caused by oscillations in the water column in the hydrostatic leveling.

The overall course of the time series is thus smoother and is less influenced by deflections caused by the measuring system, see blue curve in Figure 14.

Even though most of the loading cycles show good results, further investigations on the performance of numerical integration algorithms are necessary to be able to represent different types of deformations (static and dynamic) and different magnitudes of deflections.

Once this is done, the data acquisition can be extended to multiple sensor nodes to calculate a bending line from the computed deformations. To support this bending line calculation, further measurement quantities of the MEMS IMU should be included, *e.g.*, acceleration in the beam axis, Euler angle or quaternions.

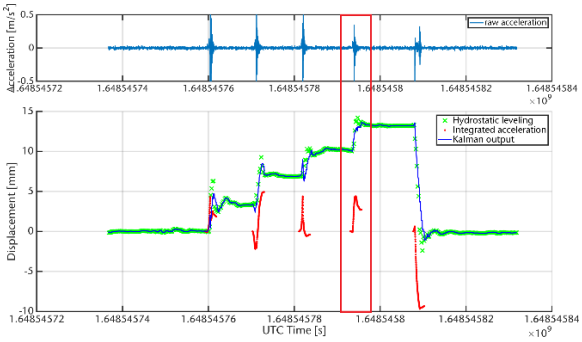

Figure 14. Result Kalman filter variant B – Fusion of integration and position – hydrostatic leveling (green); Kalman output (blue); numerical integration (red).

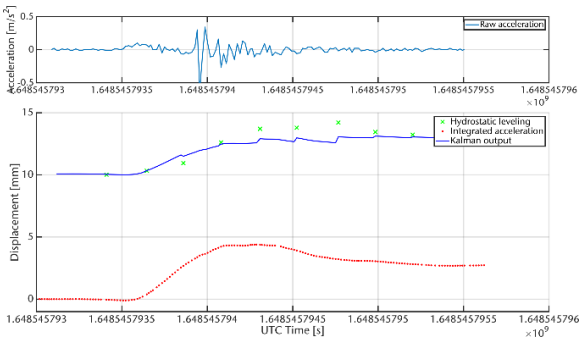

Figure 15. Result Kalman filter variant B – Selection. The Kalman output is updated by but not fully dependent on the position measurement – hydrostatic leveling (green); Kalman output (blue); numerical integration (red).

V. Conclusions

In this paper, a sensor fusion between a hydrostatic leveling system and a consumer grade MEMS accelerometer was investigated on a special test rig. The experiment shows that the hydrostatic leveling system provides accurate measurements when static loads are applied. However, the measurements are inaccurate in the moments of dynamic load. A possible approach for the enhancement of the is presented in the addition of a MEMS accelerometer.

Two variants of a Kalman filter were presented for data fusion. Variant A was used in the past by (Omidalizarandi, 2020) and (Štebe *et al.*, 2021) under different boundary conditions. Different from this paper, both authors made use an IATS for the 1D CUPT, the types of deformation and load were different, and the objective of (Omidalizarandi, 2020) was to determine the modal parameters of the bridge. For this specific load and sensor combination, variant A is less suitable because the hydrostatic leveling provides inaccurate results at times of dynamic loading.

Variant B shows promising results, since the drift of the accelerometer measurements is reduced by the double integration in the ambient window and thus the

dependency on a 1D CUPT is reduced. In particular, when the hydrostatic leveling units provide inaccurate measurements while the double integrated acceleration data can describe the deformation adequately.

The other integration algorithms have to be investigated with respect to their influence on the filter approach. Also under review in future work is the identification of dynamic load periods by means of the acceleration measurements to judge the hydrostatic leveling data in the same period.

In the future, a reference measurement needs to be included that can capture the deformation behavior during dynamic loading in particular, for example a profile scanner.

References

Bosch Sensortec (2016). BNO055 Datasheet. Available in: https://www.bosch-sensortec.com/media/boschsensortec/downloads/datasheets/bst-bno055-ds000.pdf. Accessed 30 March 2022.

Gindy, M., Nassif, H.H., and Velde, J. (2007). Bridge Displacement Estimates from Measured Acceleration Records. In: *Transportation Research Record* Vol. 2028(1), pp. 136–145.

Gindy, M., Vaccaro, R., Nassif, H., and Velde, J. (2008). A State-Space Approach for Deriving Bridge Displacement from Acceleration. In: *Computer-aided Civil Eng* Vol. 23(4), pp. 281–290.

Haupt, M., and Hesse, C, (2019). Präzise Bauwerksüberwachungsmessung mittels automatischer Druckschlauchwaage – Ein Bericht aus der Praxis. In: *GeoMonitoring* Vol. 7.

Kalman, R.E. (1960). A New Approach to Linear Filtering and Prediction Problems. In: *ASME–Journal of Basic Engineering* Vol. 82(1), pp. 35–45.

Kemkes, E., Rüffer, J., Omidalizarandi, M., Diener, D., Paffenholz, J.-A., and Neumann, I. (2019). Ein neues Verfahren zum MEMS-basierten Brückenmonitoring - Zielsetzung und Statusbericht. In: *GeoMonitoring* Vol. 7.

Omidalizarandi M. (2020). Robust Deformation Monitoring of Bridge Structures Using MEMS Accelerometers and Image-Assisted Total Stations. Dissertation, Hannover.

Omidalizarandi, M., Neumann, I., Kemkes, E., Kargoll, B., Diener, D., Rüffer, J., and Paffenholz, J.-A. (2019). MEMS based bridge monitoring supported by image-assisted total station. In: *Int. Arch. Photogramm. Remote Sens. Spatial Inf. Sci. XLII-4/W18*, pp. 833–842.

Paffenholz J.-A, (2012). *Direct geo-referencing of 3D point clouds with 3D positioning sensors*. PhD thesis. DGK, München.

Pleuger L. (2020). Beschleunigungssensoren aus dem low-cost Segment und Schlauchwaagen im Kontext des Infrastrukturmonitorings. Masterthesis, Clausthal-Zellerfeld.

Position Control (2022). Technisches Datenblatt Sensor-Typ: PC-HSA4-500. Available in: https://www.position-control.de/wp-content/uploads/2019/05/Datasheet_PC_HSD4_STANDARD.pdf. Accessed 30 March 2022.

Rauch, H.E., Tung, F., and Striebel, C.T. (1965). Maximum likelihood estimates of linear dynamic systems. In: *AIAA Journal* Vol. 3(8), pp. 1445–1450.

Resnik, B. (2014). Dynamische Belastungstests von tragenden Konstruktionen mithilfe von Beschleunigungsaufnehmern. In: *Allgemeine Vermessungs-Nachrichten* (AVN) 121(4), pp. 141–148.

Schill, F., and Eichhorn, A. (2019). Deformation Monitoring of Railway Bridges with a Profile Laser Scanner. In: *zfv* (2/2019), 109–118.

Statista (2021). Zustand der Brücken an Bundesfernstraßen in Deutschland im Jahr 2021. Bundesanstalt für Straßenwesen. Available in: https://de.statista.com/statistik/daten/studie/166122/umfrage/zustand-der-strassenbruecken-in-deutschland/.

Štebe, G., Krapež, P., Podobnik, J., and Kogoj, D. (2021). Trajectory tracking of an oscillating movement with a low-cost IMU in geodetic surveying applications. In: *Measurement* Vol. 176, pp. 109–207.

Wenner M., Meyer-Westphal M., Herbrand M., and Ullerich C. (2021). The concept of digital twin to revolutionise infrastructure maintenance: the pilot project smartBRIDGE Hamburg. In: *ITS World Congress* Vol. 27, Hamburg, Germany.